



Green Synthesis and Characterization of Antibacterial Studies by Iron Oxide Nanoparticles using *Carica papaya* Leaf Extract

¹USHA, V; ¹AMUTHA, E; ¹PUSHPALAKSMI, E; ¹JENSON SAMRAJ, J;
²RAJADURAI PANDIAN, S; ²GANDHIMATHI, S; ^{*1}ANNADURAI, G

¹Division of Nanoscience, Sri Paramakalyani Centre for Excellence in Environmental Sciences, Manonmaniam Sundaranar University, Alwarkurichi - 627 412, India.

²Sri Paramakalyani College, Department of Chemistry, Alwarkurichi - 627412, India.

*Corresponding Author Email: gannadurai@msuniv.ac.in

ABSTRACT: In present years, the synthesis of iron oxide nanoparticles (IONPs) has established excessive potential in biological applications due to their non-toxic role in biological systems, biocompatibility, and biodegradability. Ongoing research efforts focused on IONPs in the expansion of novel technologies as they can be synthesized with surface modification. Here we have studied the antibacterial effects of IONPs which were synthesized effectively through a green synthesis route by using leaf extract of the *Carica papaya* plant. The formation of IONPs was confirmed by the color change. The crystallinity of IONPs was determined by XRD and the morphology by using SEM, which showed spherical particles of well-dispersed size. The absorption peak was determined by UV-vis spectroscopy at 390 nm. Average particle size distribution was obtained at 56 nm using PSA. FL spectroscopy indicated the higher emission wavelength by redshift at 641.6 nm. TGA showed that the IONPs are thermally stable up to 200°C with no decomposition. The outcome would pave a way for utilizing IONPs for better biomedical application.

DOI: <https://dx.doi.org/10.4314/jasem.v26i3.8>

Open Access Article: (<https://pkp.sfu.ca/ojs/>) This an open access article distributed under the Creative Commons Attribution License (CCL), which permits unrestricted use, distribution, and reproduction in any medium, provided the original work is properly cited.

Impact factor: <http://sjifactor.com/passport.php?id=21082>

Google Analytics: <https://www.ajol.info/stats/bdf07303d34706088ffffbc8a92c9c1491b12470>

Copyright: Copyright © 2022 Usha *et al.*

Dates: Received: 23 August 2021; Revised: 21 December 2021; Accepted: 15 March 2022

Keywords: Nanoparticles, Green synthesis, Antibacterial, Gram-positive, Gram-negative bacteria.

Nowadays Magnetic nanoparticles have paid more attention as they are widely utilized for different applications (Khiriya *et al.*, 2020). Based on the manipulations done by magnetic fields, IOMNPs are concerned for various biomedicine and bioanalytical uses such as magnetic resonance imaging (MRI) (Ankamwar *et al.*, 2010) magnetic assays (Tartaj *et al.*, 2003), drug delivery (Saikia *et al.*, 2016), cell separation, and detection (Gu *et al.*, 2006; Lu *et al.*, 2007), treatment for hyperthermia (Zhang and Song, 2016). IOMNPs are increasingly utilized for diagnostic needs in terms of vaccine production (Rezaei *et al.*, 2019) for targeted drug/gene delivery (Shen *et al.*, 2018) and antibacterial activity against various bacteria (Ismail *et al.*, 2015). The spread of infectious diseases such as viruses and bacteria has become a challenge to public health, particularly with the rise of bacterial strains resistant to antibiotics. Production of alternative antibiotics has become one of the most significant research works to enhance the resistivity of antibiotics (Khayat sarkar and Khayat Sarkar, 2011). Generally, gram-positive and gram-negative bacterial strains can cause human diseases. On the other hand, various metal oxide nanoparticles

were found good inhibitors for different bacterial strains due to their high surface-to-volume ratio. Hence, more reactive oxygen species (ROS) and free radicals are generated and the nanoparticle can closely interact with microbial membranes by inhibiting their structure and neutralize bacteria (Andre *et al.*, 2009; Mahmoudi *et al.*, 2011). Moreover, metal oxide nanoparticles can be synthesized with enormously high surface areas and rare crystalline morphologies with a high number of edges and corners and other possibly reactive spots (Stoimenov *et al.*, 2002). Gabrielyan *et al.*, (2019) have reported the comparable antibacterial activity and action mechanisms of silver and iron oxide nanoparticles using *Escherichia coli* and *Salmonella typhimurium* and the results showed that the iron oxide NPs have proved different effects on Gram-negative and Gram-positive bacteria. Because the processes of Gram-positive and Gram-negative bacteria's cell walls have distinct paths for NPs adsorption, Gram-positive *E. hirae* showed more exposure to NPs than Gram-negative *E. coli*. However, citric acid-coated iron oxide NPs reveal more distinct antibacterial activity than iron oxide NPs treated by oleic acid at a similar concentration. The highest

*Corresponding Author Email: gannadurai@msuniv.ac.in

inhibitory effect of oleic acid-coated iron oxide NPs has been observed at the $500 \mu\text{g mL}^{-1}$ concentration (Gabrielyan *et al.*, 2020). Moreover, citric acid does not display any effect on the growth rates of examined bacteria. Antibiotic-carrier nanosystems are desirable in recent years due to the emergence of highly resistant bacterial strains and the reduced substitutions to traditional antibiotics (Hussein-Al-Ali *et al.*, 2014). EI Zowalaty *et al.*, (2015) have demonstrated the iron oxide NPs functionalized with Chitosan have been used as carriers of streptomycin. As a physical combination, this antibiotic showed a quick release within 20 min in phosphate-buffered saline, while in the form of a nanosystem its complete release was observed only after 350 min, signifying the capability of iron oxide NPs to act in controlled drug release. Huang and Hainfeld, (2013) reported the different groups of antibiotics such as rifamycin, fluoroquinolone; anthracycline, cephalosporin, and tetracycline were assured by physical adsorption to silver NPs doped iron oxide NPs. This was possible due to positively charged silver NPs binds electrostatically with the iron oxide NPs, consenting to the link of these antibiotics. Therefore, IOMNPs are proved physically and chemically stable, biocompatible, and environmentally safe, thus offering inimitable features for biomedical applications. However, when the phases of iron oxide NPs (magnetite or maghemite) reach smaller sizes (10–20 nm), superparamagnetic uses become obvious, so that the particles could reach a better performance for most of the above-mentioned applications (Run *et al.*, 2017; Rumenapp *et al.*, 2012).

MATERIALS AND METHODS



Fig 1: Green synthesis of IONPs from *Carica papaya* leaf extract

Antibacterial Property: Agar Well Diffusion Assay: The antibacterial property of the Iron oxide NPs was determined by using the bacterial species including the pathogenic bacteria such as Gram-positive

Chemicals, Reagents, and Media: Analytical grade Ferric chloride (FeCl_3) was purchased from Sigma Aldrich Pvt Ltd, India. Bacterial isolates, Gram-positive *Staphylococcus aureus* and *Bacillus subtilis*, and Gram-negative *Escherichia coli*, *Enterobacter* and *Pseudomonas fluorescens* were procured from standard vendors.

Collection of Plant Samples and Preparation of Carica papaya Extracts: The papaya plant (*Carica papaya*) leaves were collected from SPKCEES-MS University campus, Alwarkurichi. The fresh leaves were then washed multiple times with tap water followed by distilled water. The leaves were then dried in an oven for an hour and then ground to form a fine powder. 5 grams of fine powders are boiled with 100 ml of deionized water at 80°C for 30 min and the extract is then filtered using Whatman No. 1 filter paper. The filtrate was stored at 40°C for further use.

Green synthesis of Fe_2O_3 nanoparticles: Ferric chloride (FeCl_3) was used as the precursor for the synthesis of the Fe_2O_3 nanoparticles. 20 mL of the papaya leaves extract was added dropwise with 80 mL of 0.1M FeCl_3 solution at room temperature as shown in Fig.1. The resultant mixture was stirred using a magnetic stirrer for 30 min and the formation of intense brown colored solution confirmed the synthesis of iron oxide nanoparticles. The nanoparticles were separated by centrifugation at 6000 rpm for 20 min and cleansed by subsequent washing with ethanol and water about 2-3 times. The NPs were finally dried in a hot air oven at 80°C for 3 hr and calcinated for 400°C .

Staphylococcus aureus (a) and *Bacillus subtilis* (b), and Gram-negative *Escherichia coli* (c), *Enterobacter* (d), and *Pseudomonas fluorescens* (e), by the well diffusion method. The different concentrations used

were at 0.1 mg and 0.5 mg for the identification of antimicrobial activity of the above bacterial species. All the plates were incubated at 37°C for 24 hours, and the zone of inhibition of bacteria was measured.

RESULTS AND DISCUSSIONS

X-ray diffraction Analysis: Analysis of structure and crystalline size of the synthesized Iron oxide NPs was carried out by XRD pattern. XRD patterns of the synthesized Iron oxide NPs samples are shown in Fig. 1. The XRD patterns reveal that all the samples are a single phase in nature. The XRD analysis of synthesized Iron oxide NPs from leaf extract showed diffraction peaks at 30.4°, 35.7°, 43.3°, 53.6°, 57.3° and 63.0° respectively. When compared with the standard, the obtained XRD spectrum confirmed that the synthesized Iron oxide NPs were in nanocrystal form and crystalline (Rumenapp *et al.*, 2012; Gabrielyan *et al.*, 2019). The peaks can be assigned to the planes (220), (311), (400), (422), (511), and (440) facets of an iron crystal, respectively. The same result was reported by Brice *et al.* (2009) and indicates that the iron nanoparticles are crystalline (correlated to JCPDS card: number 19-629 and 39-1346). The Full Width at Half Maximum (FWHM) values was used to calculate the size of the nanoparticles. The average size of Iron oxide NPs nanoparticles synthesized from leaf extract was calculated using Scherrer's equation where Scherrer's constant value 94 was selected due to the crystalline nature of the nanoparticles. The average sizes of the synthesized nanoparticles from leaf extract were found to be 43 nm, respectively.

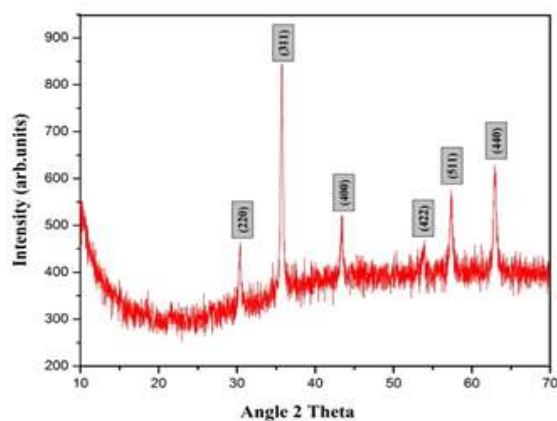


Fig 2: XRD pattern of green synthesized IONPs

Scanning Electron Microscopy: The Scanning Electron Microscopic analysis was performed using Carl Zeiss Evo 18 Secondary Electron Microscope with the magnification from 25 KX–40 KX depending on the sample. The morphology of IOMNPs was characterized by SEM indicated the agglomerated spherical nanoparticles as shown in Fig. 3. The

agglomerated nanoparticles are due to the solution form of the sample and improper drying on the electric slab (SardarSiddiqueUrRahman *et al.*, 2017). The spherical shapes are observed within the size range of 200 nm (Iwamoto and Ishigaki, 2013).

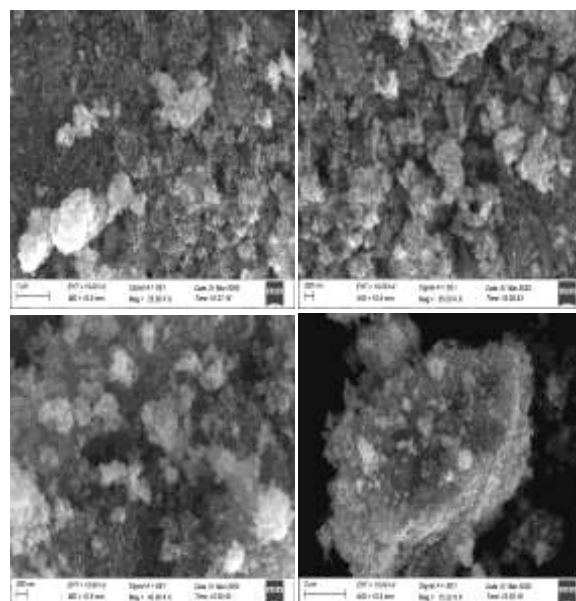


Fig 3: SEM Image of the green synthesized IONPs

UV-Visible spectroscopy (UV-Vis): The reduction of Iron oxide magnetic nanoparticles was monitored by using a double beam UV-vis spectrophotometer (Perkin Elmer, Singapore) of the reaction medium in the wavelength range of 300–600 nm with a 1000 mm quartz cell. The resolution of the UV-vis spectrophotometer was 1 nm. The graph of wavelength on the X-axis and absorbance on the Y-axis was plotted (Zhang and Song, 2016). The optical properties of Iron oxide NPs were studied by UV-vis spectrophotometer in a range of wavelength from 200 to 1200 nm as shown in Fig. 4. The absorption peak of Iron oxide NPs appeared at 390 nm indicates the formation of Iron oxide NPs. The broad peak corresponds to the synthesized Iron oxide NPs and the small peak observed in the UV region may be due to the small organic molecules present in the reaction mixture.

Fourier Transform Infra-Red Spectroscopy: FT-IR spectrum of synthesized iron oxide NPs was carried out to identify the groups responsible for the capping and stabilization of nanoparticles. The FTIR spectrum of iron oxide NPs was shown in Fig. 5. The peaks at 3435 cm^{-1} represent the O–H stretch, H-bonded alcohols, and phenols. The peak at 2924 cm^{-1} and 2921 cm^{-1} corresponds for C–H stretch alkanes (Gu *et al.*, 2006; Lu *et al.*, 2007). The absorption peak of 1669

cm^{-1} might be due to C=O stretch carbonyls (general). The peaks at around 1210 cm^{-1} and 1070 cm^{-1} represent the C–N stretch aliphatic amines. 985 correspond to =C–H bends alkenes. The peaks around 832 cm^{-1} for C–Cl stretch alkyl halides, 548 cm^{-1} for C–Br stretch alkyl halides as shown in Table.1.

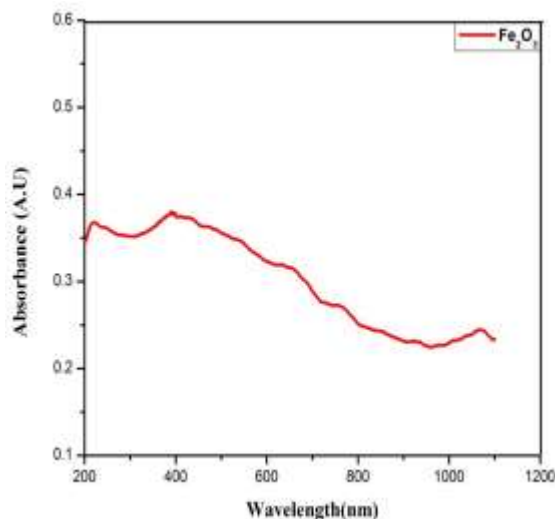


Fig 4: UV-Vis Spectra of the green synthesized IONPs

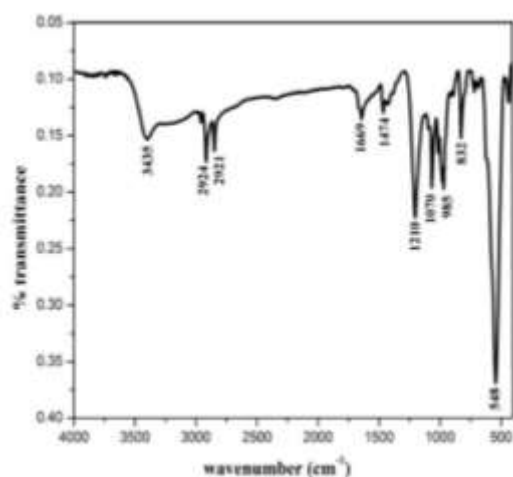


Fig 5: FTIR spectrum of green synthesized IONPs

Table 1: Peak table of IONPs

S. No	Peak (cm^{-1})	Functional Group
1	3435	O–H stretch, H–bonded alcohols, phenols
2	2924	C–H stretch alkanes
3	2921	C–H stretch alkanes
4	1669	C=O stretch carbonyls (general)
5	1210	C–N stretch aliphatic amines
6	1070	C–N stretch aliphatic amines
7	985	=C–H bend alkenes
8	832	C–Cl stretch alkyl halides
9	548	C–Br stretch alkyl halides

Particle Size Distribution (PSD): PSD study was performed by using Dynamic Light Scattering (DLS) technique to analyze particle size and their dispersity of IOMNPs. DLS is based on the laser diffraction

method with multiple scattering techniques employed to study the average particle size of nanoparticles. The prepared sample was dispersed in deionized water followed by ultra-sonication. Then the solution was filtered and centrifuged for 15 min at 25°C with 5000 rpm and the supernatant was collected (Stoimenov *et al.*, 2002).. The supernatant was diluted 4-5 times and the particle distribution in the liquid was studied in a computer-controlled particle size analyzer (*ZETA sizer Nanoseries, Malvern instrument Nano Zs*). The size distribution of the Iron oxide NPs was measured by Dynamic Light Scattering (DLS). The DLS method examines the intensity of scattered light passing through a solution of nanoparticles. The average size was measured from the majority of particle sizes of a sample. From the result, the average size distribution of the synthesized Iron oxide NPs was observed at 56 nm as shown in Fig. 6.

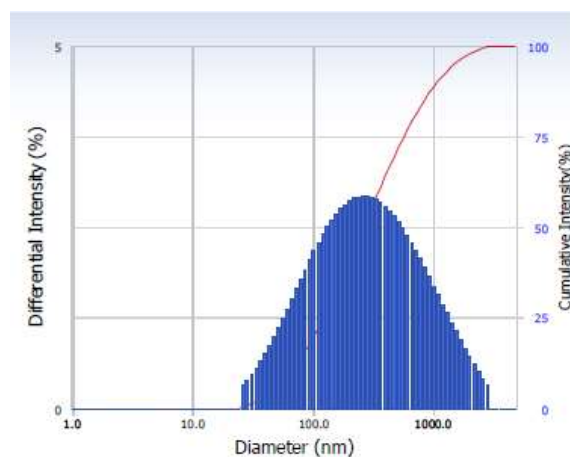


Fig 6: The particle size distribution of the green synthesized IONPs

Fluorescence Spectroscopy (FL): Fluorescence spectra of Iron oxide NPs were performed using an Instrument model LS45. Fluorescence spectra of Iron oxide NPs were recorded at room temperature by a Fluorescence spectrophotometer. Measurements were made over the wavelength range of 400-900 nm. Intensities of maximum wavelength emissions were collected from the experiments, and the emission values were plotted as wavelength (nm) vs Intensity (A.U). Fig. 7 shows two characteristic peaks of Iron oxide NPs. The lower emission peak was attributed at 362.8 nm representing the Iron oxide NPs formation and a higher emission peak was measured with an excitation wavelength of 641.6 nm may attribute to the surface defects. The fluorescence spectra were the most preferable technique for investigating energy levels (Susanne Mertens *et al.*, 2019). An increase in fluorescence intensity with increasing iron oxide nanoparticles size was observed.

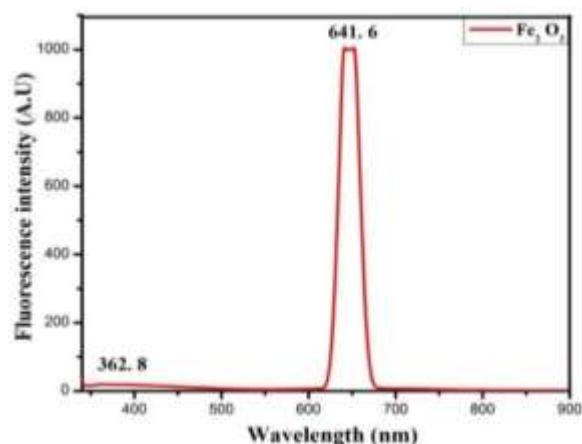


Fig 7: Fluorescence spectra of green synthesized IONPs

Thermogravimetric Analysis: TGA is considered the most important method for studying the thermal stability of polymers and nanoparticles. The thermal stability of Iron oxide NPs was investigated by using TG/DTA (*Hitachi-Thermo Gravimetry/Differential Thermal Analyzer STA7000*, Japan). TGA analysis was performed from 100°C to 500°C with a heating rate of 10°C/min under nitrogen flow as shown in Fig. 8. The DTA curve shows a strong exothermic peak at 55.4 Cel (-11.69 mg) possibly corresponding to the lattice deformation of Iron oxide NPs or release of nitrate and acetate ion. The second weight loss was observed at 205.9 Cel (-11.96 mg) which was attributed to the decomposition of water and CO physically adsorbed on the oxide surface (Karami, 2010). A sharp weight loss of -12.13 mg at 496.5 Cel was observed. The endothermic peak observed in the DTA curve was less than 100°C. The first peak was a weak exothermic peak which appeared between 280 to 400°C and was assigned to a direct transition of Maghemite to Hematite and the second exothermic peak at 500°C was assigned to a transition Hematite to Magnetite.

Antibacterial Activity: The different species of bacteria showed a zone of inhibition in the well diffusion method of antimicrobial activity (OlenaIvashchenko, 2015). The different patterns of the zone of inhibitions were observed in Fig. 9 and 10. Synthesized Iron oxide nanoparticles showed antibacterial activity against both Gram-positive and negative bacteria. Pathogenic bacteria are grown in nutrient broth and a 24 h culture of these strains was swabbed uniformly onto the individual plates containing Muller-Hinton Agar (MHA) using sterile cotton swabs. About 5 wells were made and the purified Iron oxide NPs at different weights like 0.1 mg and 0.5 mg were added into each well on all plates and penicillin was used as control (Gabrielyan *et al.*,

2020) as shown in Table 2. The plates were incubated for 24 h at 37°C in an incubator. After incubation, the different levels of zone formation around the well were measured.

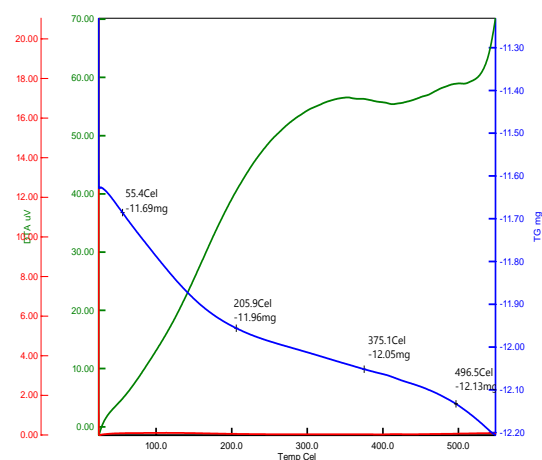


Fig 8: TGA graph of green synthesized IONPs

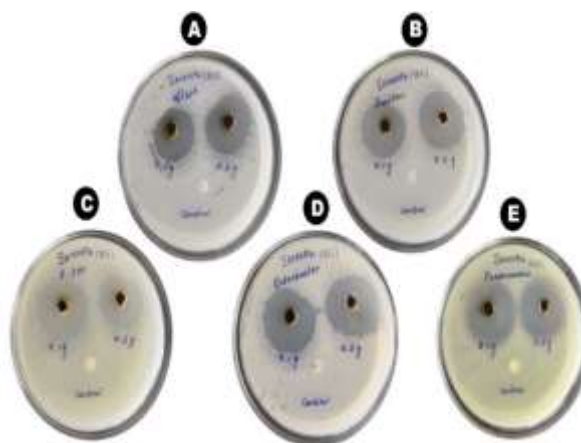


Fig 9: Antibacterial properties of green synthesized IONPs

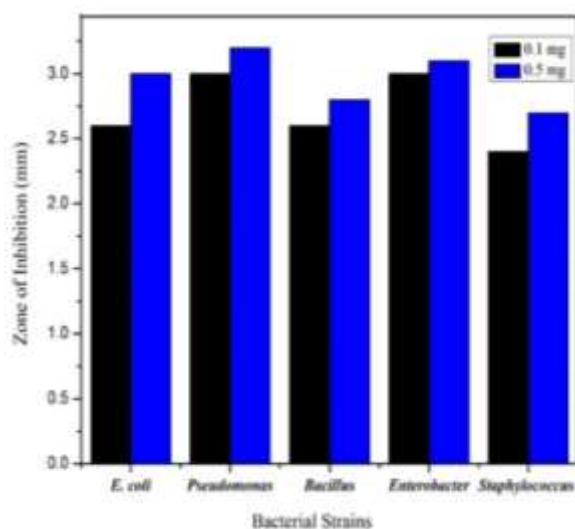


Fig 10: Bar graph of the green synthesized IONPs

USHA, V; AMUTHA, E; PUSHPALAKSMI, E; JENSON SAMRAJ, J; RAJADURAI PANDIAN, S; GANDHIMATHI, S; ANNADURAI, G

Table 2: Antibacterial activity of IONPs

Concentration	Zone of Inhibition (mm in diameter)				
	<i>Bacillus sp</i>	<i>E. coli</i>	<i>Enterobacter</i>	<i>Staphylococcus aureus</i>	<i>Pseudomonas</i>
0.1 mg	2.6	2.6	3	2.4	3
0.5 mg	2.8	3	3.1	2.7	3.2
Control	-	-	-	-	-

Conclusions: The present investigation dealt with the iron oxide nanoparticle was synthesized effectively through a green synthesis route by using the leaf extract of the *Carica papaya* plant. The synthesized IONPs are characterized by X-Ray Diffraction (XRD), Scanning Electron Microscopy (SEM), Fourier Transform Infra-Red Spectroscopy (FT-IR), UV-visible spectroscopy (UV-vis), Fluorescence spectroscopy (FL), Particle Size Distribution (PSD), and Thermogravimetric analysis (TGA). From the characterized result, structural, optical, and thermal properties of IONPs were confirmed. Therefore, synthesizing IONPs could serve as an excellent application in the antibacterial studies that would help to design various antibodies for untreatable microbes.

REFERENCES

- Andre, E; Lutz Madler, L; Darrell, V; Tian, X; Eric, M; Hoek, V (2009). Understanding biophysicochemical interactions at the nano--bio interface. *Nat. Mater.* 8(7): 543–557
- Ankamwar, BTC; Lai, JH; Huang, RS; Liu, M; Hsiao, CH; Chen, YK (2010). Biocompatibility of Fe₃O₄ nanoparticles evaluated by in vitro cytotoxicity assays using normal, glia and breast cancer cells. *Nanotechnology.* 21(7):7510
- Brice SE, Alford CW, Cowart, LA (2009). Modulation of sphingolipid metabolism by the phosphatidylinositol-4-phosphate phosphatase Sac1p through regulation of phosphatidylinositol in *Saccharomyces cerevisiae*. *J Biol Chem.* 284(12):7588-96
- El Zowalaty, ME; Al Ali, SHH; Hussein, MI; Geilich, BM; Webster, TJ; Hussein, MZ (2015). The ability of streptomycin-loaded chitosan-coated magnetic nanocomposites to possess antimicrobial and antituberculosis activities. *Int. J. Nanomedicine.* 10: 3269-3372
- Gabrielyan, L; Badalyan, H; Gevorgyan, V; Trchounian, A (2020). Comparable antibacterial effects and action mechanisms of silver and iron oxide nanoparticles on *Escherichia coli* and *Salmonella typhimurium*. *Sci. Rep.* 0123456789: 1–12
- Gabrielyan, L; Hovhannisyan, A; Gevorgyan, V; Ananyan, M; Trchounian, A (2019). Antibacterial effects of iron oxide (Fe₃O₄) nanoparticles: distinguishing concentration-dependent effects with different bacterial cells growth and membrane-associated mechanisms. *Appl. Microbiol. Biotechnol.* 103(6): 2773–2782, 2019
- Gu, H; Xu, K; Xu, C; Xu, B (2006). Biofunctional magnetic nanoparticles for protein separation and pathogen detection. *Chem. Commun.* 9:941–949
- Huang, HS; Hainfeld, JF (2013). Intravenous magnetic nanoparticle cancer hyperthermia. *Int. J. Nanomedicine.* 8: 2521-2524
- Hussein-Al-Ali, SH; El Zowalaty, ME; Hussein, MZ; Ismail, M; Webster, TJ (2014). Synthesis, characterization, controlled release, and antibacterial studies of a novel streptomycin chitosan magnetic nanoantibiotic. *Int. J. Nanomedicine.* 9: 549-562.
- Ismail, RA; Sulaiman, GM; Abdulrahman, SA; Marzoog, TR (2015). Antibacterial activity of magnetic iron oxide nanoparticles synthesized by laser ablation in liquid. *Mater. Sci. Eng. C.* 53:286–297
- Iwamoto T; Ishigaki, T (2013). Fabrication of iron oxide nanoparticles using laser ablation in liquids. *J. Phys. Conf. Ser.* 441: 012034
- Karami, H (2010). Synthesis and characterization of iron oxide nanoparticles by solid state chemical reaction method. *J. Clust. Sci.* 21(1): 11–20
- Khayat Sarkar Z; Khayat Sarkar, F (2011). Synthesis and Magnetic Properties Investigations of Fe₃O₄. *Nanoparticles.* 7(4):197–200
- Khiriya, PK; Moradiya, M; Khare, PS (2020). Facile synthesis of high magnetization long term stable bimetallic FeCo nanoparticles. *Int. J. Nano Dimens.* 11(3): 299–302
- Lu, AH; Salabas, E; Schuth, F (2007). Magnetic nanoparticles: synthesis, protection, functionalization, and application. *Angew. Chemie Int. Ed.* 46(8): 1222–1244
- USHA, V; AMUTHA, E; PUSHPALAKSMI, E; JENSON SAMRAJ, J; RAJADURAIPANDIAN, S; GANDHIMATHI, S; ANNADURAI, G

- Mahmoudi, M; Lynch, I; Ejtehadi, MR; Monopoli, MP; Bombelli, FB; Laurent, S (2011). Protein-nanoparticle interactions: opportunities and challenges. *Chem. Rev.* 111(9):5610–5637
- Olenaivashchenko, ML, Barbara, P, Marcin, J, Grzegorz, N, Maciej, W, KarolZalęski, TB, Alicja WS (2015). Synthesis and characterization of magnetite/silver/antibiotic nanocomposites for targeted antimicrobial therapy. *Mater. Sci. Eng. C.* 55: 343–359
- Rezaei, M; Hosseini, SN; Khavari-Nejad, RA; Najafi, F; Mahdavi, M (2019). HBs antigen and mannose loading on the surface of iron oxide nanoparticles in order to immuno-targeting: fabrication, characterization, cellular and humoral immunoassay. *Artif. Cells, Nanomedicine, Biotechnol.* 47(1): 1543–1558
- Rumenapp, C; Gleich, B; Haase, A (2012), Magnetic Nanoparticles in Magnetic Resonance Imaging and Diagnostics. *Pharm. Res.* 29: 1165–1179
- Run, L; Yuancheng, LT; MacDonald, HW; James, P; Xingui, P; Jing, H; Liya W; Andrew, YW; Jianyong, Y; Hui, M (2017). Improving sensitivity and specificity of capturing and detecting targeted cancer cells with anti-biofouling polymer coated magnetic iron oxide nanoparticles. *Colloids Surfaces B Biointerfaces.* 150, 261–270
- Saikia, C; Das, MK; Ramteke, A; Maji, TK (2016). Effect of crosslinker on drug delivery properties of curcumin loaded starch coated iron oxide nanoparticles. *Int. J. Biol. Macromol.* 93: 1121–1132m
- Sardar, SU, Muhammad, T, Qureshia, K, Sultanaa, W, Rehmanbe, MY, Khanc, MH, Asifd, M, Farooqa, NS (2017). Single step growth of iron oxide nanoparticles and their use as glucose biosensor. *Results Phys.* 7: 4451–4456
- Shen, L; Li, B; Qiao, Y (2018). Fe₃ O₄ Nanoparticles in Targeted Drug/Gene Delivery Systems. *Mater.* (Basel, Switzerland).11(2):324-326
- Stoimenov, PK; Klinger, RL; Marchin, GL; Klabunde, KJ (2002). Metal oxide nanoparticles as bactericidal agents. *Langmuir.* 18(17): 6679–6686
- Susanne, M, Antonio, A, Konra, A, Tobias, B, Luca, B, Tim, B, Marco, C, David, F, Carlo, F, Thibaut, H, Anton, H, Marc. K, Thierry, L, Peter, L, MicheleManotti, IvanPeric, DavidC. Radford, Daniel, S, Martin, S, Kathrin, V, Joachim, W, Sascha, W. (2019). A novel detector system for KATRIN to search for keV-scale sterile neutrinos. *J. Phys. G Nucl. Part. Phys.* 46(6): 65203
- Tartaj, P; Del Puerto Morales, M; Veintemillas - Verdaguer, S; Gonzalez-Carreno, T; Serna, CJ (2003). The preparation of magnetic nanoparticles for applications in biomedicine. *J. Phys. D. Appl. Phys.* 36(13): 179-182
- Zhang, ZQ; Song, SC (2016). Thermosensitive/superparamagnetic iron oxide nanoparticle-loaded nanocapsule hydrogels for multiple cancer hyperthermia. *Biomaterials.* 106:13–23